SoftwareX 27 (2024) 101672

Contents lists available at ScienceDirect

SoftwareX

journal homepage: www.elsevier.com/locate/softx

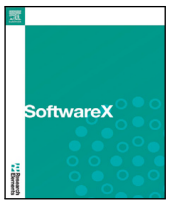

Software update

MCRAD: A *Monte Carlo* photon transport code for analysis of fluorescence and elastic scattering diagnostics

Joshua M. Herzog *, Volker Sick

Department of Mechanical Engineering, University of Michigan, 2350 Hayward St., Ann Arbor, MI 48109, USA

ARTICLE INFO

Dataset link: https://github.com/jmherzog-umich/MCRAD

Keywords:
Monte Carlo
Radiative transfer
Laser-induced fluorescence
Radiative trapping

ABSTRACT

Radiative transfer, or the propagation of radiation (light) through a system, is an important problem in imaging and optical diagnostics in complex media including turbulent gas flows, biological tissues, and particle suspensions. *Monte Carlo* (MC) methods are the *de facto* standard for radiative transfer simulation in complex media. While many sophisticated tools exist within this domain, few are well-suited to investigating laser- and fluorescence-imaging in turbid media. Here, a fast MC code for investigating light propagation in turbid media is presented. This tool is intended to enable detailed, physics-based analysis of laser and imaging techniques of simple model systems for use in experimental design and interpretation.

Code metadata

Current code version	v0.1.0
Permanent link to code/repository used for this code version	https://github.com/ElsevierSoftwareX/SOFTX-D-23-00844
Legal Code License	GPL-3.0
Code versioning system used	git
Software code languages, tools, and services used	C++
Compilation requirements, operating environments & dependencies	C++17 compliant compiler and C++ standard library (*e.g.*, GCC 7 with libstdc++)
Support email for questions	jmherzog@umich.edu

1. Motivation and significance

Broadly speaking, absolute luminescence or fluorescence quantum yield (FQY) from bulk samples, especially in granular or powdered media, is an important parameter in many fields of analytical chemistry in both the life sciences and physical sciences despite the well-known inherent measurement difficulty [1]. Indeed, typical laboratory procedures advise taking steps to minimize scattering in quantitative spectroscopy measurements [2]. However, in many cases it is not feasible to avoid these effects such as in particle-based flow diagnostics (*e.g.*, thermographic phosphor thermometry [3–5]), in imaging of turbulent flows, imaging through a turbulent atmosphere [6], and imaging of cell suspensions or tissues [7]. The presence of even small amounts of scattering in fluorescence spectroscopy measurements also poses a significant challenge for analysis of chemical composition [8], and in laboratory characterization of laser dyes and other luminescent chemicals [9]. These effects can be especially important for quantitative imaging experiments where radiative transfer (RT) effects (*e.g.*, multiple scattering and reabsorption) can alter the signal-to-noise and signal-to-background ratios of the measurement [10].

Radiative transfer is a complicated physical phenomena that describes the propagation of electromagnetic radiation through a medium. Analytical solutions to the RT equation are not possible in most cases, and even for the simplest cases require numerical solutions to integral equations. Many of these solutions were derived by Chandrasekhar [11]. Although Chandrasekhar's solutions provide a means to calculate properties of light propagation through plane films, in practice determination of even the simplest quantities such as reflection coefficient is cumbersome. *Monte Carlo* (MC) methods are widely considered the *de facto* standard for RT problems [12] since they are theoretically exact (neglecting statistical errors) given appropriate microscopic scattering models. However, they can be difficult to implement for scientists

DOI of original article: https://doi.org/10.1016/j.jqsrt.2024.109063.
* Corresponding author.
E-mail address: jmherzog@umich.edu (Joshua M. Herzog).

https://doi.org/10.1016/j.softx.2024.101672
Received 19 December 2023; Received in revised form 15 February 2024; Accepted 21 February 2024
Available online 7 June 2024

without a strong physics, statistics, and computer science background. Improved tools and methods to analyze RT effects in optical diagnostics are needed.

Several widely-used implementations of the MC method for radiative transfer exist including MCNP [13], MCML [14], and Multi-Scattering [15]. MCNP is a flexible general MC code that is intended primarily for nuclear physics including charged and neutral particle interactions. MCML is a popular multi-layer MC code that analyzes energy deposition through layered plane-parallel media. Finally, Multi-scattering is an online platform that analyzes laser propagation in particulate media, *e.g.*, suspensions of spherical particles. Some studies have developed MC methods that incorporate fluorescence analysis in the past [16], but this capability does not appear to be widely available, especially in the context of laser diagnostics and quantitative luminescence or fluorescence analysis.

Here we report on the development of MCRAD. MCRAD implements the MC method for simple geometries with a focus on analysis of experiments, and fluorescence imaging of turbid media in particular. The code is capable of performing accurate fluorescence analysis in both quasi-static and time-resolved cases. MCRAD has experimental support for saturation of absorption transitions and image simulation. MCRAD provides the imaging and diagnostics communities a simple, easy to use tool to investigate scattering and other RT effects in experiments.

2. Software description

MCRAD is a RT code that implements the MC method in both quasi-static and time-dependent modes. A primary focus of MCRAD compared to similar codes is the focus on quantifying luminescence or fluorescence emission from bulk samples for diagnostic applications. A detailed description of the MC method for RT is given in [17], and a detailed description of the application of the MC method to fluorescence emission is given in [18]. A brief overview of the MC method is as follows.

A set of photon packets are generated randomly based on input beam parameters. Then, each packet is propagated through the simulation stochastically. Displacement is determined by sampling the exponential distribution, packets are displaced to the interaction location, and the new packet direction is sampled randomly from the scattering phase function. At each interaction location, the packet weight is reduced accordingly and absorption, transmission, and scattering intensities are scored. Fluorescence photons are generated following absorption and are propagated in a similar fashion. In single-photon mode, the weight of each photon packet is unity and the entire packet is either absorbed, transmitted, or scattered in whole at each interaction. Time-resolved simulations are implemented in a similar fashion, but photon packets are only propagated up to the current simulation time at each step, ensuring that all photon packets are temporally synchronized. The simulation ends when all photons packets have been terminated, or following a predetermined number of steps. A diagram illustrating the procedure is shown in Fig. 1.

Several quantities are scored in the simulation: ballistic transmission, specular reflection, scattered light intensity (diffuse reflection and transmission), and fluorescence emission intensity. These quantities are illustrated in Fig. 1. Time- and angle-resolved intensities are also recorded for these quantities. Irradiance, absorption, fluorescence reabsorption, and fluorescence irradiance are also scored on grids within the simulation domain, and optionally can be time-resolved. Both cylindrical and Cartesian geometries are implemented. In particular, this software enables a researcher to investigate how microscopic properties of fluorescent scattering particles (*e.g.*, biological cells or phosphors) behave in bulk, and how particle density, albedo, scattering anisotropy, and slab geometry impact macroscopically observable fluorescence. Several additional features are experimental including polychromatic physics, image simulation, and saturation of absorption transitions. Interference of wave packets is also experimental and uses differences

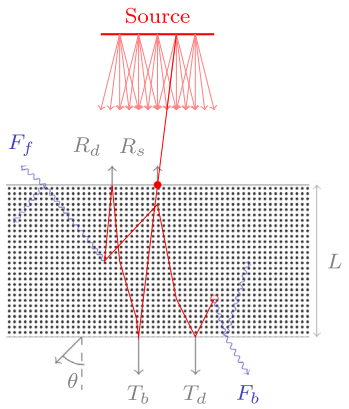

Fig. 1. Illustration of the incident, reflected, transmitted, and fluorescence intensities in MCRAD. The quantities R_d, R_s, T_d, T_b, F_f, and F_b represent the diffuse reflection, specular reflection, diffuse transmission, ballistic transmission, front-face fluorescence emission, and back-face fluorescence emission coefficients, respectively.

in propagation distance to model, e.g., thin film interference in the absence of scattering. However, MCRAD does not consider wave optics effects introduced by the simulation geometry. Small slab widths can introduce wavelength-dependent diffraction effects which are not modeled here. Finally, FQY is assumed constant for simplicity, but future developments are planned to enable a wavelength-dependent FQY to simulate, *e.g.*, multiple electronic transitions.

Additional planned future developments include parallelization using a distributed memory approach (*e.g.*, with MPI), uncertainty analysis, and a more comprehensive selection of spectral lineshapes and cross-section models. While runtimes are relatively short on typical desktop computers for most simulations, MC simulations of this nature are embarassingly parallel. Parallelization can greatly reduce runtime, improve convergence especially for trace quantities, and enable simultaneous repeated simulations for uncertainty analysis. Parallelization additionally can enable rapid spectral analysis by simultaneously considering multiple wavelength sources in parallel. Other planned improvements include point, sheet, and other source profiles, improved polychromatic analysis, and spatially-varying scattering properties.

2.1. Single-photon, time-resolved fluorescence simulation

The primary use case of MCRAD is time-resolved fluorescence analysis using single-photon mode. At every interaction location, the photon packet is either scattered or absorbed in whole. Following absorption, a new photon packet is generated at the same location, but at the (randomly-sampled) fluorescence wavelength with weight given by the product of the incident photon weight and the FQY. The photon emission time delay and direction are randomly sampled from an exponential and uniform distribution to simulate an exponential decay rate and isotropic emission, respectively. The fluorescence photons are then propagated in an identical fashion to the incident photon packets.

The time-step algorithm is illustrated in Fig. 2. For each photon packet, an initial interaction distance λ is randomly sampled based on the Beer–Lambert law. At each step, the packet is propagated forward along its path until (1) it is transmitted or reflected at a wall, (2) it reaches a distance λ and is scattered or absorbed, or (3) it propagates for a duration equal to the propagation time step. If the photon is transmitted or absorbed, the propagation ends; if the photon is reflected or scattered, the direction is updated, λ is decremented or resampled, and the process is repeated. If the photon survives after propagating a distance corresponding to the simulation time step, the step is complete and the iteration for this packet ends. Scored quantities are updated at the end of each photon propagation step. In this way, all photon

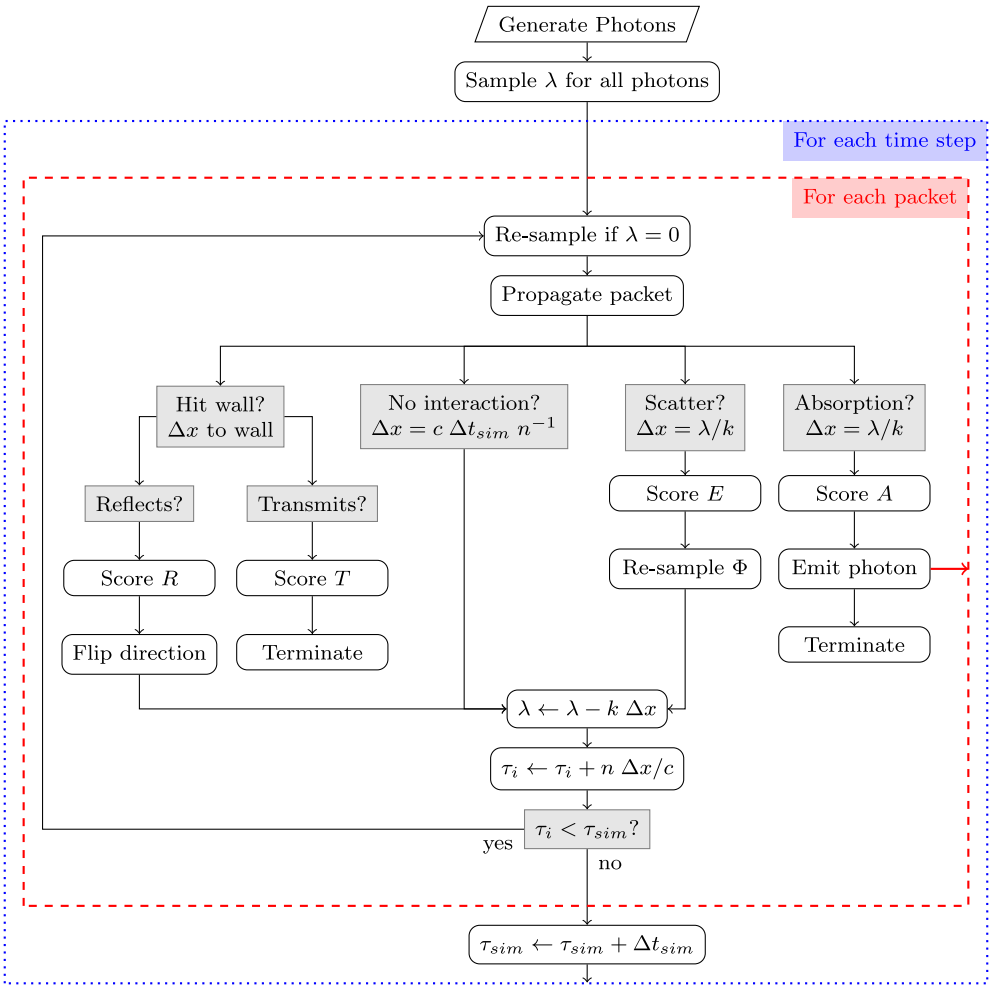

Fig. 2. Diagram of the time-resolved, single-photon *Monte Carlo* algorithm as implemented in MCRAD. Fluorescence photons are added to the photon packet queue and are treated identically, but scores are separated for fluorescence analysis. The symbols λ, τ, k, c, and n represent the optical path length, photon time, extinction coefficient, speed of light, and refractive index, respectively. Finally, λ_i represents the optical path length of the photon which is incremented through the time step i, which tracks the completion of the iteration, Δx is the physical displacement before the next interaction, and Δt is the simulation time step.

packets are synchronized and scored quantities are accurate within the simulation time step.

After a photon is absorbed, a fluorescence photon is generated in the same location with a randomly sampled direction, wavelength, and emission time as described previously. Absorption is assumed to happen entirely at the interaction location (rather than uniformly along the path length), consistent with single-photon packets. Since the fluorescence photon time is typically much larger than the current simulation time, the packet is ignored until the simulation reaches the fluorescence packet time; from that point on, the fluorescence packet is propagated identically to the incident packets. If no photons are being propagated but there are still fluorescence photons with emission times larger than the current simulation time, the simulation time is incremented to the earliest fluorescence photon time. A second time step is used for time-resolved output of fluorescence quantities to account for differences in time scales. However, this second time step does not alter the simulation fidelity in this mode.

2.2. Gridded fluorescence simulation

A simplified fluorescence analysis mode based on a Cartesian or cylindrical grid is also implemented to enable, *e.g.*, laser-induced fluorescence simulations. In this mode, incident photons are propagated through the system to determine local energy deposition on a predetermined grid to simulate, *e.g.*, a laser sheet. Following the excitation portion of the simulation, fluorescence photon packets are generated on the grid randomly based on the energy deposition calculation. Since the grid is sampled randomly, the fluorescence portion of the simulation depends on the selected grid resolution. This mode is intended to analyze absorption and fluorescence separately. Time-resolved gridded fluorescence simulations, in which fluorescence is generated during the excitation process rather than after, are implemented as an experimental feature in the current release.

2.3. Uncertainty analysis

Detailed uncertainty analysis should be performed by repeating simulations. Uncertainty analysis is also planned to be incorporated and performed automatically in the future via parallelization. However, as intensity values are calculated from the number of observations of a discrete random event (Poisson process), uncertainties are straightforward to estimate for most quantities. The uncertainty (standard deviation) of any intensity value x is

$$\sigma_x = \sqrt{x_0 x} \tag{1}$$

where x_0 is the contribution of a single photon packet to x. For example, if 10^7 photon packets are used in the simulation, $x_0 = 10^{-7}$ for the reflection, absorption, transmission, and fluorescence coefficients. Note that for scaled quantities (*e.g.*, incident fluence), the value of x_0 needs to be scaled accordingly.

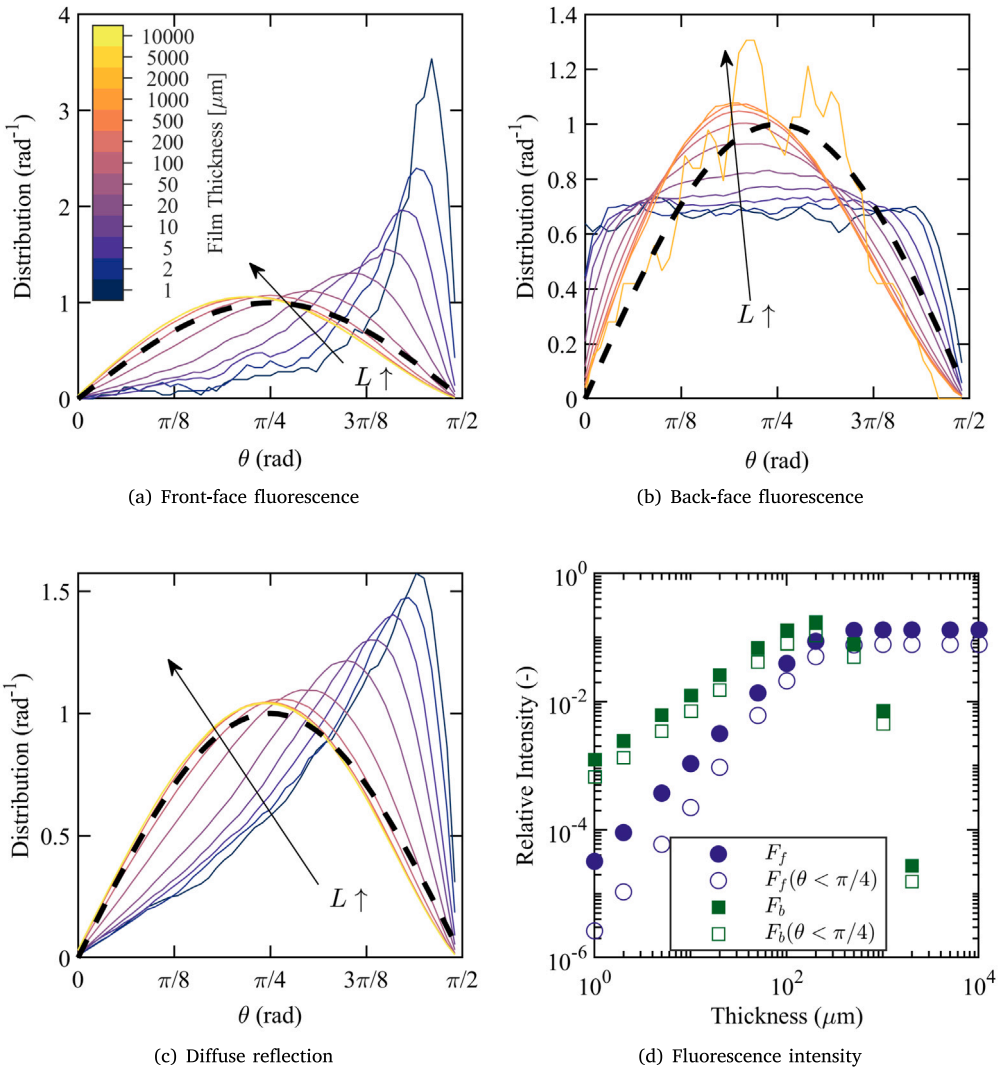

(a) Front-face fluorescence

(b) Back-face fluorescence

(c) Diffuse reflection

(d) Fluorescence intensity

Fig. 3. Calculated fluorescence and diffuse reflection angular distributions and total fluorescence intensity from an *E. coli* biofilm of varying thickness. F_f, F_b, and R_d represent fluorescence emission escaping the front (incident) surface, fluorescence emission escaping the rear surface, and diffuse reflection, respectively. The dashed black curve represents the Lambert-Cosine distribution.

3. Illustrative examples

MCRAD was used to investigate *en face* or front-face fluorescence emission from *E. coli* biofilms with near-ultraviolet (370 nm) excitation. The *E. coli* cells are assumed to have a scattering cross-section of 1 μm, albedo $\alpha = 0.9975$, cell density of 0.5 μm^{-3} and scattering anisotropy $g = 0.98$ using the Henyey–Greenstein phase function [19]. Several illustrative results are plotted in Fig. 3 including the total fluorescence intensity F_f and F_b emitted from the front and back faces of the samples (Fig. 3(d)), respectively, and the angular distributions of diffuse reflection and fluorescence (Figs. 3(a), 3(b), and 3(c)) for several smear thicknesses. For comparison, the approximation of Lambert's Cosine law is superimposed. Lambert's cosine law states that diffuse reflectance or emission intensity is proportional to the cosine of the incidence angle. When integrated over solid-angle, the expression becomes

$$\frac{I_0}{\pi}\int \cos(\theta)\, d\Omega = 2I_0 \int \sin(\theta)\cos(\theta)\, d\theta, \tag{2}$$

where I_0 is the total emitted flux and I_0/π is the peak flux emitted at normal incidence. Thus, the distribution function for comparison is

$$p(\theta) = 2\sin(\theta)\cos(\theta). \tag{3}$$

Interference effects were not included for this example; however, they are expected to be negligible based on the assumed geometry.

Briefly, the data show some interesting features related to fluorescence angular distributions. For thin films characterized here by $L \lessapprox 100$ μm, we observe that the fluorescence and reflection distributions are non-Lambertian. The back-face fluorescence intensity distribution is approximately flat, while the front-face fluorescence and reflection distributions are strongly peaked towards high incidence angles. We similarly observe the transition towards the Lambertian regime as L increases beyond 100 μm. However, notably, all of the quantities deviate from Lambert's Cosine law. Imaging and spectroscopy measurements, which typically use small collection solid-angles due to optical limitations, could be impacted by these behaviors. Finally, we observe that the peak relative front-face fluorescence intensity is around 0.1 for thick films. This measure is an effective quantum yield for the biofilm; for every N incident excitation photons used in the experiment, we expect to observe at most $0.1N$ fluorescence photons from the front-face. This is a key parameter for diagnostic design that determines imaging performance and equipment requirements that is otherwise difficult to quantify.

These results illustrate a primary use case for MCRAD. The program can be used to quantify the performance of a fluorescence imaging

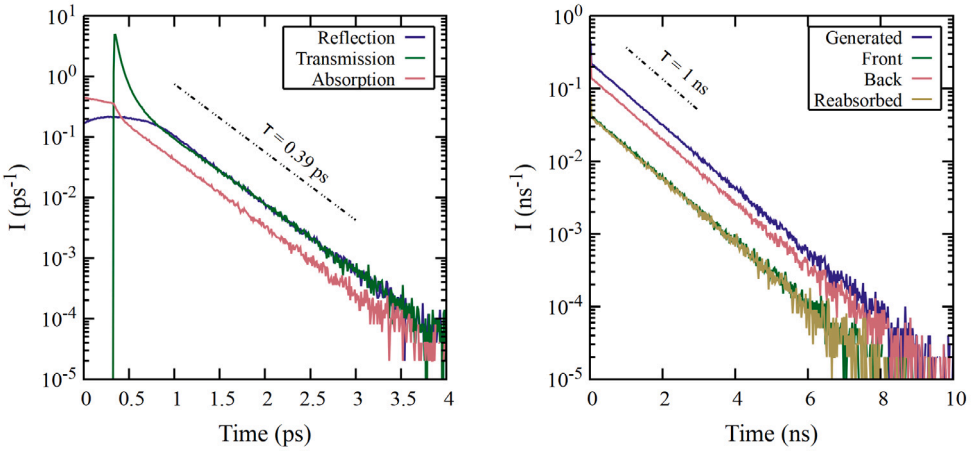

(a) 100 μm incident (b) 100 μm fluorescence

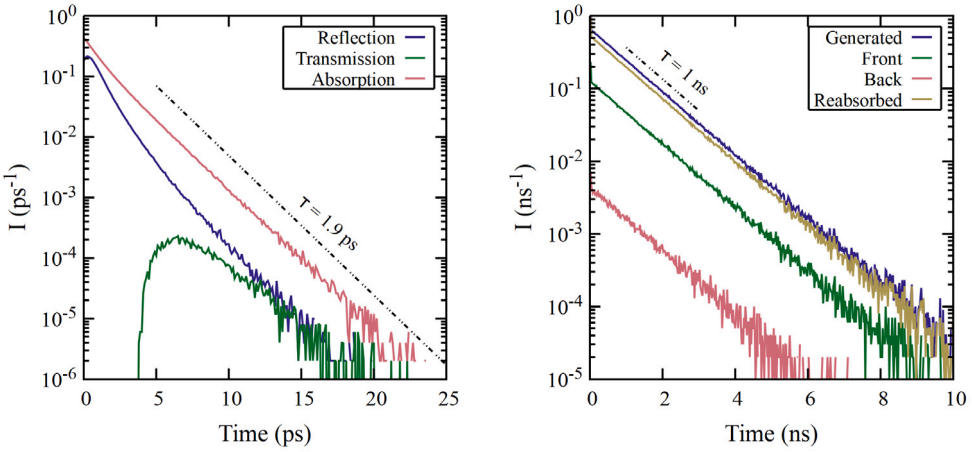

(c) 1000 μm incident (d) 1000 μm fluorescence

Fig. 4. Time-resolved absorption, transmission, reflection, and fluorescence profiles for 100 and 1000 μm thick biofilm for a 1 ns intrinsic fluorescence lifetime. Fluctuations in the temporal profiles are consistent with the Poisson process analysis as described in Section 2.3.

or spectroscopy tool, to aid in analysis of data, and to optimize diagnostic design. For example, the sample results show that for thin *E. coli* biofilms, it is advantageous to collect fluorescence emission on the back face of the biofilm, rather than the front face, to maximize fluorescence intensity for trace detection. Similarly, due to the strong scattering anisotropy of the *E. coli* cells, front-face fluorescence and diffuse reflection imaging would likely require large collection solid-angles to feasibly image thin films. This suggests that alternative excitation wavelengths or collection strategies may be advantageous.

3.1. Time-resolved single-photon fluorescence simulation

A time-resolved simulation was additionally run for two film thicknesses of 100 and 1000 μm, respectively, and the results are plotted in Fig. 4. The fluorescence intensity decay curves plotted in Figs. 4(b) and 4(d) show that there is little impact on the intrinsic fluorescence decay lifetime of 1 ns for the chosen conditions. Comparing the transmission profiles in Figs. 4(a) and 4(c), the characteristic timescale of the diffusive transmission and reflection is on the order of 0.4 ps for the 100 μm thick film, but closer to 2 ps for the 1000 μm thick film. Since the intrinsic fluorescence lifetime is three orders of magnitude larger than this value, it is unsurprisingly not impacted significantly by radiative transfer.

Comparing the incident light (absorption, reflection, and transmission) profiles, we observe a significant change in behavior. The transmission curve for the 1000 μm film thickness does not appear to have a ballistic peak. Rather, the time at which the transmission intensity peaks is a result of scattering. In comparison, the thinner 100 μm thick film does exhibit a strong peak near 0.4 ps corresponding to the unattenuated photon flux. We similarly observe changes in the time-scale for the absorption and reflection processes near the ballistic transmission time. At times larger than the ballistic time (*i.e.*, after the ballistic photons exit the system), the absorption, reflection, and transmission time-scales tend to a time-scale that is related to the size and scattering properties of the system.

3.2. Wavelength-resolved fluorescence emission

One final simulation was run to demonstrate wavelength-resolved analysis. In this case, the scattering and absorption cross-sections are allowed to scale according to the Rayleigh scattering solution ($\sigma \propto \omega^4$) but have the same values at 800 THz as used previously. This results in a constant single-cell albedo. The source spectrum was changed to a normal distribution with peak of 850 THz and a 5-THz spectral width (standard deviation). The scattering anisotropy is assumed to be independent of wavelength for simplicity. The fluorescence spectrum is taken to be a normal distribution with peak of 680 THz and a width of 50 THz which roughly corresponds to the fluorescence of NADH, a common fluorophore found in bacteria cells. The spectra of the fluorescence emission at the front and back surfaces of the slab are plotted in Fig. 5 for a 100- and 1000-μm thick slab.

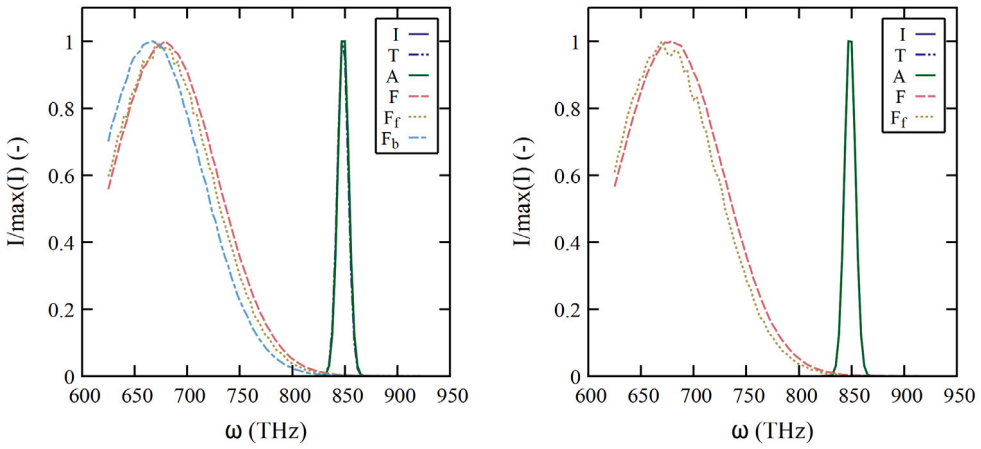

(a) 100 μm width (b) 1000 μm width

Fig. 5. Normalized excitation, transmission, and fluorescence spectra for two slab thicknesses.

While the spectra show negligible change in the transmitted laser profile in both simulations, the fluorescence spectra change appreciably with thickness, and between the front and back surfaces. In particular, for the 100 μm slab, there is a ∼20 THz shift in the peak back-face fluorescence frequency compared to the intrinsic (single-cell) fluorescence spectrum due to the combined radiative transfer effects. A similar but smaller shift is observable in the front-face fluorescence spectrum.

4. Impact

MCRAD enables researchers to quantitatively investigate fluorescence imaging and spectroscopy of dense, turbid media. In particular, MCRAD is used to investigate radiative trapping and reabsorption of fluorescence emission in dense media. This enables researchers to gain insight into the relationship between fluorescence intensity and cell or particle properties such as scattering and absorption cross-sections. MCRAD can aid in the quantitative interpretation of fluorescence imaging and spectroscopy data by taking into account the bulk scattering and radiative transfer properties of the fluorescent medium. MCRAD has recently been used in particular to illustrate that radiative transfer plays a significant role in *en face* fluorescence imaging and spectroscopy of bacterial suspensions and smears [20], such that accurate interpretation of data requires careful consideration of cell properties. Based on this conclusion, additional investigations to characterize quantitatively the optical properties of a range of bacteria species are ongoing. Related work also used earlier versions of MCRAD to investigate the relationship between scattering albedo and absorption of bulk samples [21].

5. Conclusion

MCRAD is a fluorescence imaging and spectroscopy focused implementation of the *Monte Carlo* method for radiative transfer that is intended to aid in design, analysis, and optimization of laser and optical diagnostics for scattering media. In particular, MCRAD has been used to relate single-particle fluorescence properties to macroscopically-observable fluorescence intensities for use in quantitative fluorescence imaging of bacterial biofilms. MCRAD enables investigators to better understand how absorption and fluorescence occurs in scattering media, and to use that information to improve fluorescence-based diagnostic technologies.

CRediT authorship contribution statement

Joshua M. Herzog: Writing – review & editing, Writing – original draft, Visualization, Validation, Software, Project administration, Methodology, Investigation, Formal analysis, Data curation, Conceptualization. **Volker Sick:** Writing – review & editing, Supervision, Resources, Project administration, Funding acquisition.

Declaration of competing interest

The authors declare that they have no known competing financial interests or personal relationships that could have appeared to influence the work reported in this paper.

Data availability

The code is available open-source under the GPL3 license and is available at the following repository: https://github.com/jmherzog-umich/MCRAD.

References

[1] Tomasini EP, San Roman E, Braslavsky SE. Validation of fluorescence quantum yields for light-scattering powdered samples by laser-induced optoacoustic spectroscopy. Langmuir 2009;25(10):5861–8.
[2] Würth C, Grabolle M, Pauli J, Spieles M, Resch-Genger U. Relative and absolute determination of fluorescence quantum yields of transparent samples. Nat Protoc 2013;8(8):1535–50.
[3] Stephan M, Zentgraf F, Berrocal E, Albert B, Böhm B, Dreizler A. Multiple scattering reduction in instantaneous gas phase phosphor thermometry: Applications with dispersed seeding. Meas Sci Technol 2019;30(5):054003.
[4] Abram C, Fond B, Beyrau F. Temperature measurement techniques for gas and liquid flows using thermographic phosphor tracer particles. Prog Energy Combust Sci 2018;64:93–156.
[5] Lee H, Böhm B, Sadiki A, Dreizler A. Turbulent heat flux measurement in a non-reacting round jet, using BAM: Eu^{2+} phosphor thermography and particle image velocimetry. Appl Phys B 2016;122:1–13.
[6] Zhang P, Gong W, Shen X, Han S. Correlated imaging through atmospheric turbulence. Phys Rev A 2010;82(3):033817.
[7] Moretti C, Gigan S. Readout of fluorescence functional signals through highly scattering tissue. Nat Photon 2020;14(6):361–4.
[8] Bevilacqua M, Rinnan Å, Lund MN. Investigating challenges with scattering and inner filter effects in front-face fluorescence by PARAFAC. J Chemometrics 2020;34(9):e3286.
[9] Rohwer LS, Martin JE. Measuring the absolute quantum efficiency of luminescent materials. J Luminescence 2005;115(3–4):77–90.
[10] Berrocal E, Kristensson E, Richter M, Linne M, Aldén M. Application of structured illumination for multiple scattering suppression in planar laser imaging of dense sprays. Optics Express 2008;16(22):17870–81.

[11] Chandrasekhar S. Radiative transfer. 1st ed. New York: Dover Publications, Inc.; 1960, p. 1–393.
[12] Noebauer UM, Sim SA. Monte Carlo radiative transfer. Liv Rev Comput Astrophys 2019;5:1–103.
[13] Rising ME, Armstrong JC, Bolding SR, Brown FB, Bull JS, Burke TP, et al. MCNP® code version 6.3.0 release notes. Tech. rep. LA-UR-22-33103, Rev. 1, Los Alamos, NM, USA: Los Alamos National Laboratory; 2023, http://dx.doi.org/10.2172/1909545, URL https://www.osti.gov/biblio/1909545.
[14] Wang L, Jacques SL, Zheng L. MCML—Monte Carlo modeling of light transport in multi-layered tissues. Comput Methods Programs Biomed 1995;47(2):131–46.
[15] Jönsson J, Berrocal E. Multi-scattering software: part I: Online accelerated Monte Carlo simulation of light transport through scattering media. Opt Express 2020;28(25):37612–38.
[16] Churmakov DY, Meglinski IV, Greenhalgh DA. Amending of fluorescence sensor signal localization in human skin by matching of the refractive index. J Biomed Opt 2004;9(2):339–46.
[17] Zhu C, Liu Q. Review of Monte Carlo modeling of light transport in tissues. J Biomed Opt 2013;18(5):050902.
[18] Welch A, Gardner C, Richards-Kortum R, Chan E, Criswell G, Pfefer J, et al. Propagation of fluorescent light. Lasers Surg Med: Off J Am Soc Laser Med Surg 1997;21(2):166–78.
[19] Henyey LG, Greenstein JL. Diffuse radiation in the galaxy. Astrophys J 1941;93:70–83.
[20] Herzog JM, Agosta G, Sick V. On the impact of radiative transfer in fluorescence imaging of bacterial films and suspensions. J Quant Spectrosc Radiat Transf 2024;109063.
[21] Herzog JM, Sick V. Quantitative spectroscopic characterization of near-UV/visible E. Coli (pYAC4), B. Subtilis (PY79), and green bread mold fungus fluorescence for diagnostic applications. J Fluorescence 2023;1–13.